Supporting information

Fe_3O_4/Co_3O_4 binary oxides as bifunctional electrocatalyst for rechargeable Zn-air battery by one-pot pyrolysis of zeolitic imidazolate frameworks

Zhili Wang,[a,#] Jinhui Yang,[a,b,#] Yuanting Tang,[a] Zhiping Chen,[c] Qizi Lu,[b,c] Gurong Shen,[d] Yanwei Wen,[a] Xiao Liu,*[,c] Feng Liu,[e] Rong Chen,[b,c] Bin Shan,*[,a,b]

[a] State Key Laboratory of Materials Processing and Die & Mould Technology, School of Materials Science and Engineering, Huazhong University of Science and Technology, Wuhan 430074, Hubei, People's Republic of China

[b] China-EU Institute for Clean and Renewable Energy, Huazhong University of Science and Technology, Wuhan 430074, Hubei, People's Republic of China

[c] State Key Laboratory of Digital Manufacturing Equipment and Technology, School of Mechanical Science and Engineering, Huazhong University of Science and Technology, Wuhan 430074, Hubei, People's Republic of China

[d] School of Materials Science and Engineering, Tianjin University, Tianjin 300072, People's Republic of China

[e] State Key Laboratory of Advanced Technologies for Comprehensive Utilization of Platinum Metal, Kunming Institute of Precious Metals, Kunming 650106, Yunnan, People's Republic of China

[#] Zhili Wang and Jinhui Yang contributed equally to this work.

* Corresponding authors: *xiaoliu@hust.edu.cn* (Xiao Liu), *bshan@mail.hust.edu.cn* (Bin Shan)

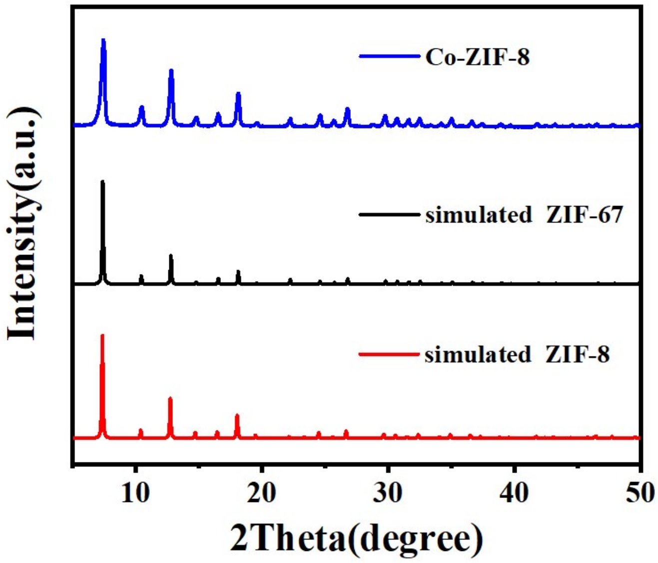

Fig. S1. XRD patterns of Co-ZIF-8, simulated ZIF-67 and simulated ZIF-8. All characteristic peaks of simulated ZIF-8 and ZIF-67 are presented in Co-ZIF-8.

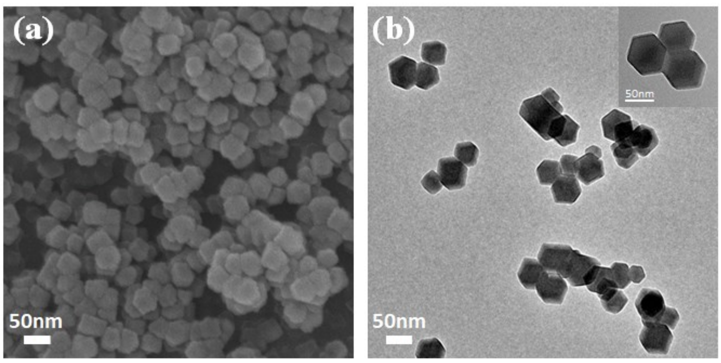

Fig. S2. (a) SEM and (b) TEM images of Co-ZIF-8. The as-prepared crystal shows the rhombododecahedral morphology.

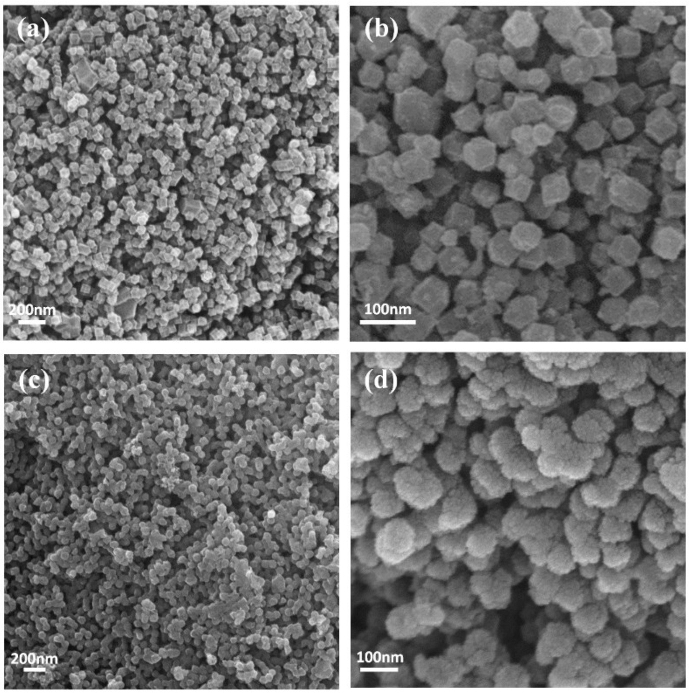

Fig. S3. SEM images of (a-b) Co_3O_4-CN and (c-d) Fe_2O_3-CN.

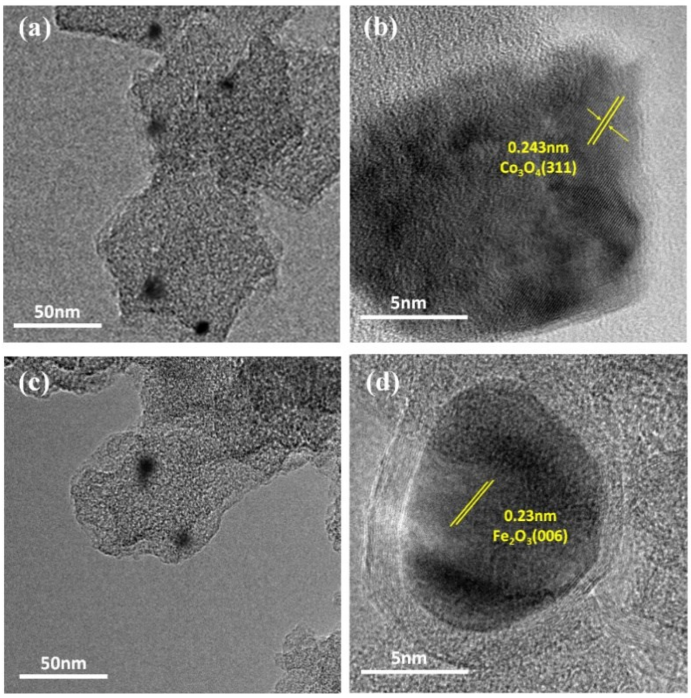

Fig. S4. TEM images of (a-b) Co_3O_4-CN and (c-d) Fe_2O_3-CN, which exhibit the domains of Co_3O_4 and Fe_2O_3 in Co_3O_4-CN and Fe_2O_3-CN catalysts, respectively.

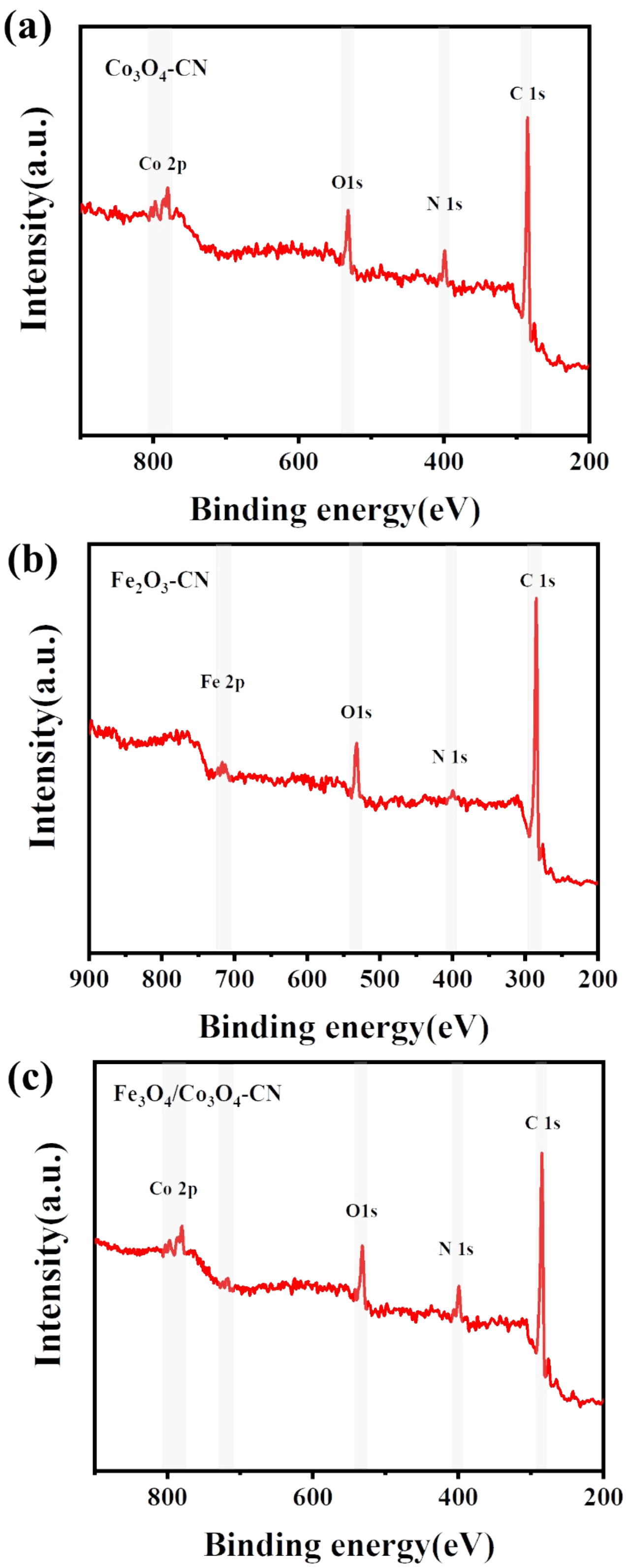

Fig. S5. XPS spectra of (a) Co_3O_4-CN, (b) Fe_2O_3-CN and (c) Fe_3O_4/Co_3O_4-CN.

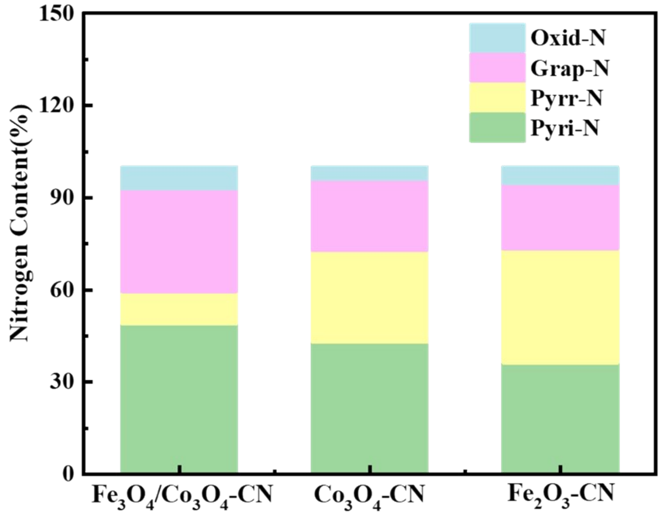

Fig. S6 The relative contents of different N types (Pyri-N, Pyrr-N, Grap-N, Oxid-N) in the prepared catalysts of Fe_3O_4/Co_3O_4-CN, Co_3O_4-CN and Fe_2O_3-CN

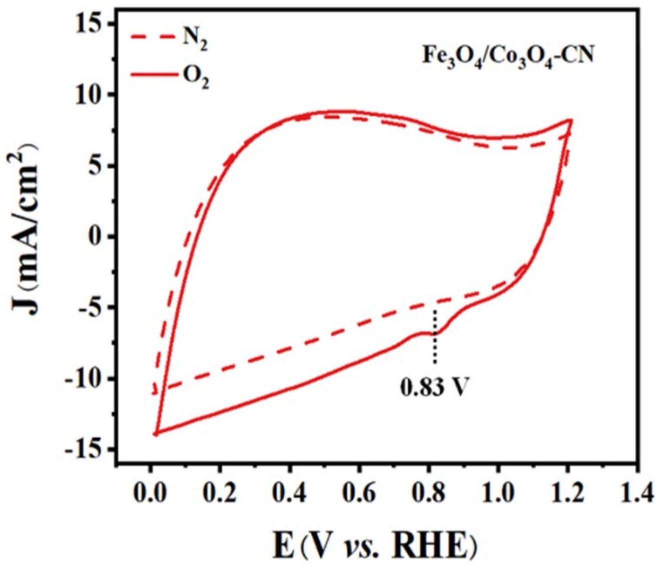

Fig. S7. CV curves for Fe_3O_4/Co_3O_4-CN in N_2 and O_2-saturated 0.1M KOH solution.

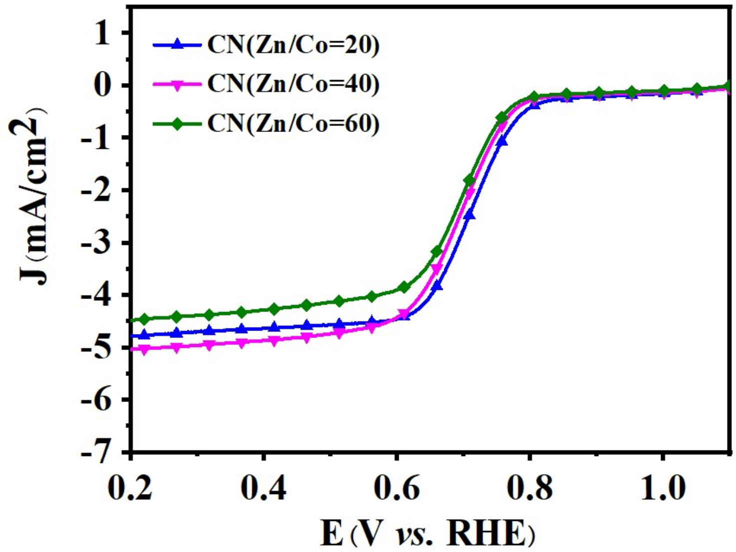

Fig. S8. LSV curves of CN obtained with different molar ratio of Zn/Co in Co-ZIF-8 at a rotating rate of 1600 rpm in O_2-saturated 0.1 M KOH solution. The molar ratio of Zn^{2+} and Co^{2+} in the solution for Co-ZIF-8 preparation has been optimized to 20:1.

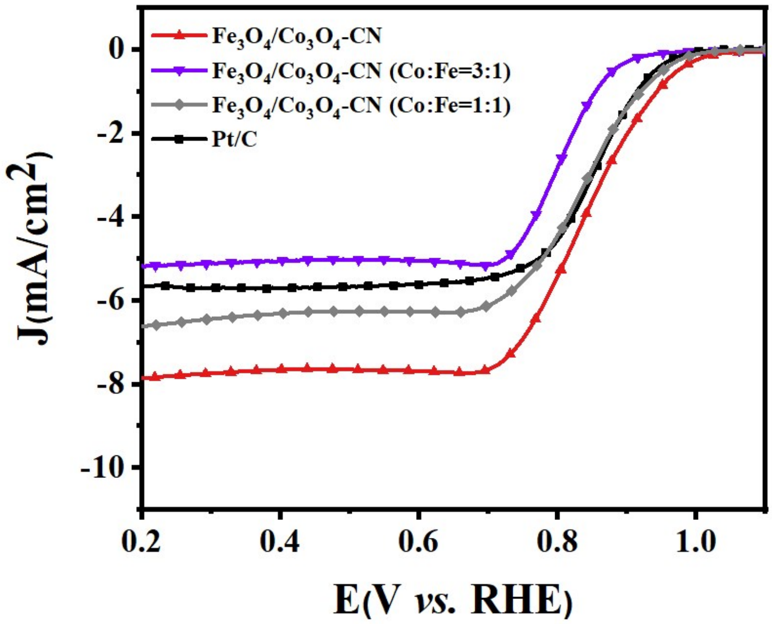

Fig. S9. LSV curves of different molar ratio of Co/Fe in Fe_3O_4/Co_3O_4-CN and Pt/C obtained at a rotating rate of 1600 rpm in O_2-saturated 0.1 M KOH solution. Co/Fe ratio of 2:1 is the optimized molar ratio in sample preparation.

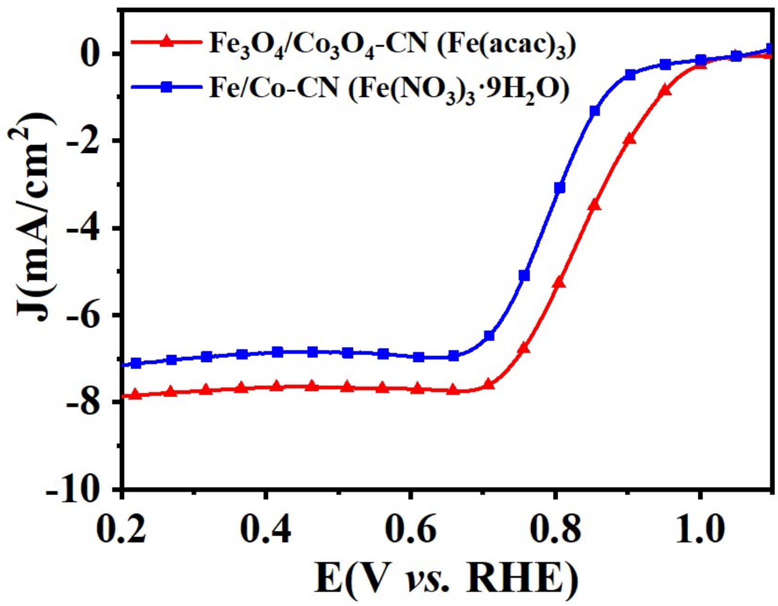

Fig. S10. LSV curves of different kind of Fe sources in Fe_3O_4/Co_3O_4-CN at a rotating rate of 1600 rpm in O_2-saturated 0.1 M KOH solution. The $Fe(acac)_3$ is better than $Fe(NO_3)_3$.

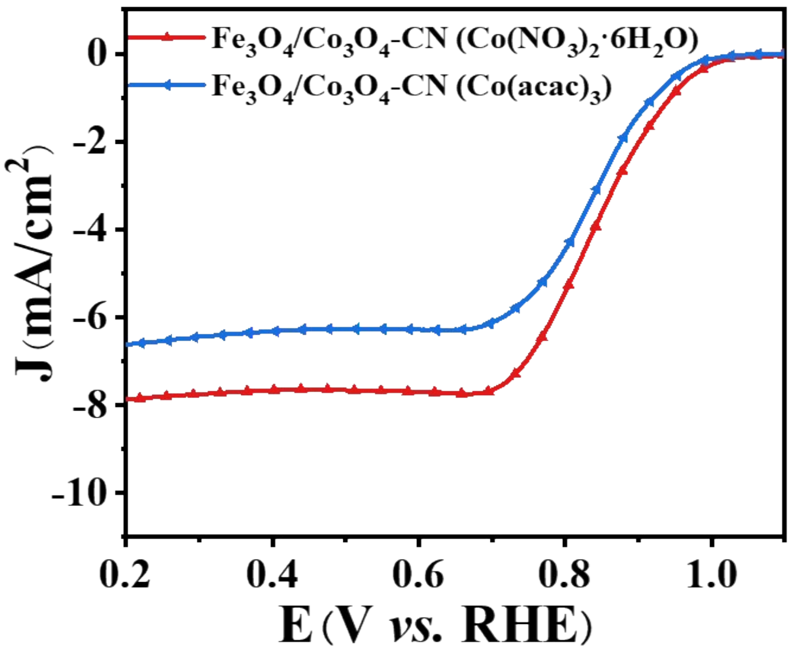

Fig. S11. LSV curves of different kind of Co sources in Fe_3O_4/Co_3O_4-CN at a rotating rate of 1600 rpm in O_2-saturated 0.1 M KOH solution. The $Co(NO_3)_2$ is better than $Co(acac)_3$.

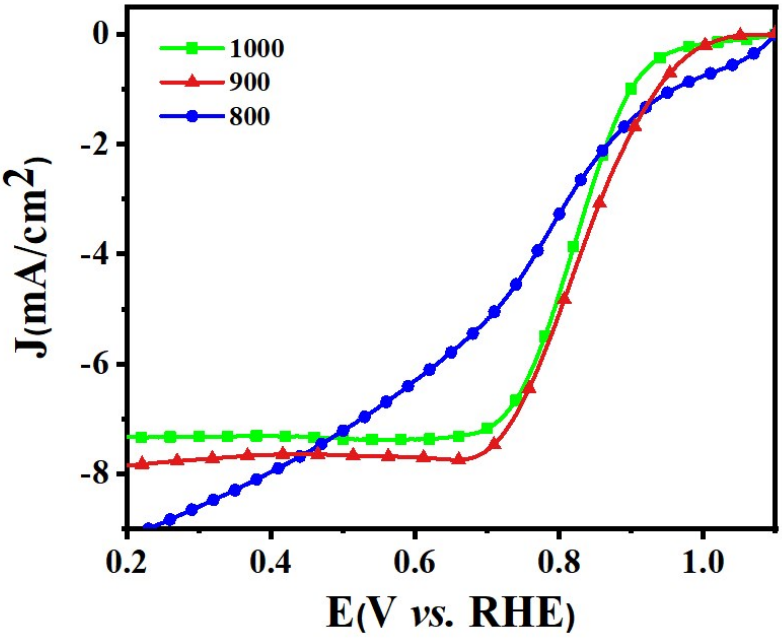

Fig. S12. LSV curves of Fe_3O_4/Co_3O_4-CN at different pyrolysis temperature of 800, 900 and 1000 ℃. The 900 ℃ is the optimization temperature for pyrolysis.

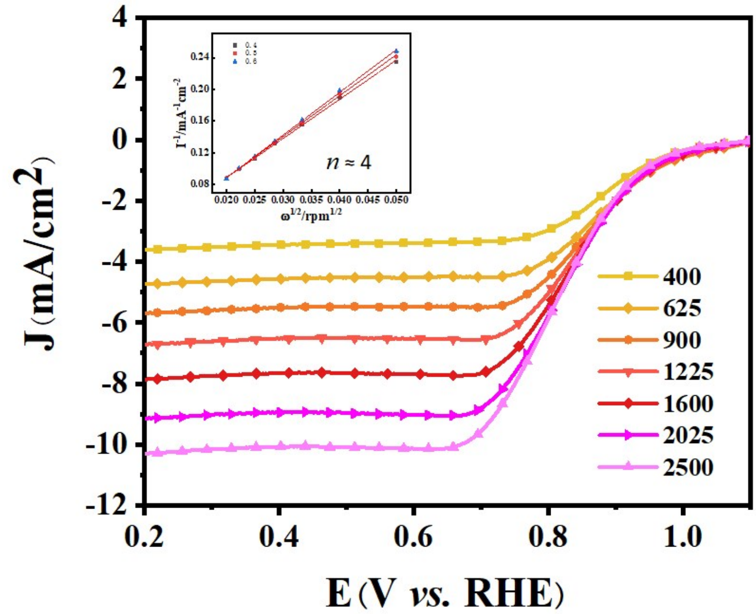

Fig. S13. LSV curves for Fe_3O_4/Co_3O_4-CN at a rotation rate from 400 to 2500 rpm. The corresponding Koutechy−Levich plots at various disk potentials are inserted. The electron transfer number calculated by K-L equation is consist with the result of H_2O_2 yields test.

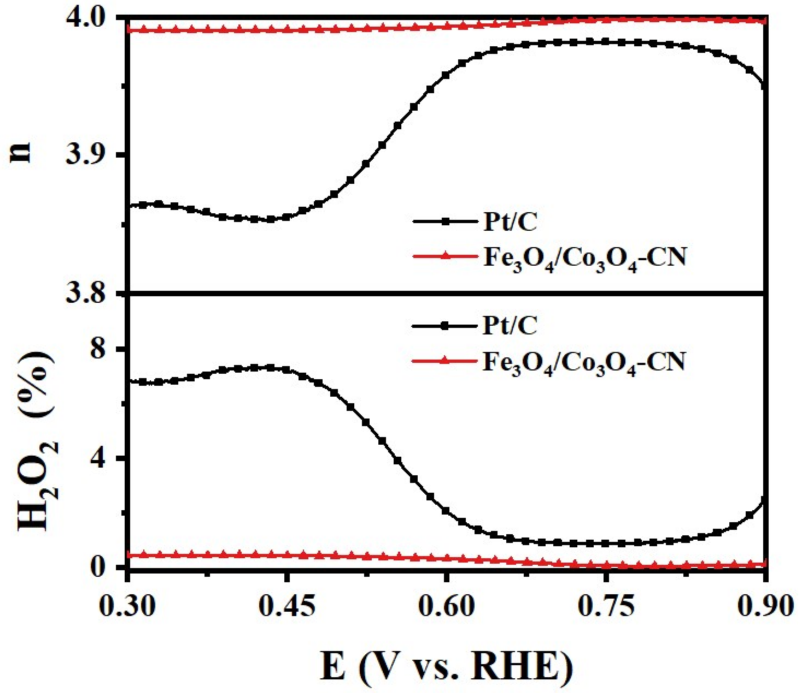

Fig. S14. The numbers of electron transfer and H_2O_2 yields of Fe_3O_4/Co_3O_4-CN catalyst and commercial Pt/C.

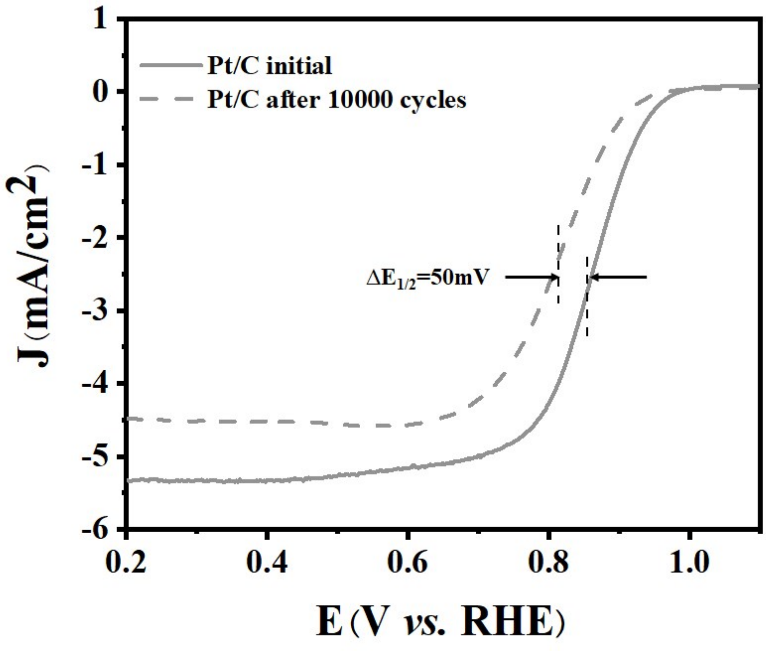

Fig. S15. ORR polarization curves of the Pt/C before and after 10000 potential cycles between 0.6 and 1.0 V versus RHE with a scan rate of 50 mV s^{-1} in O_2-saturated 0.1 M KOH solution.

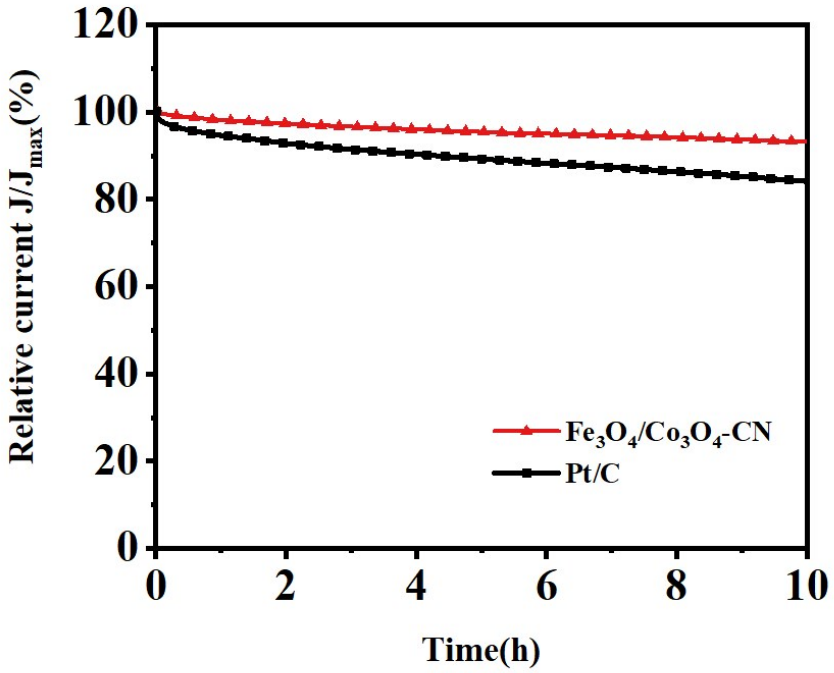

Fig. S16. Chronoamperometric response of Fe_3O_4/Co_3O_4-CN and Pt/C at 0.6 V for 10 h.

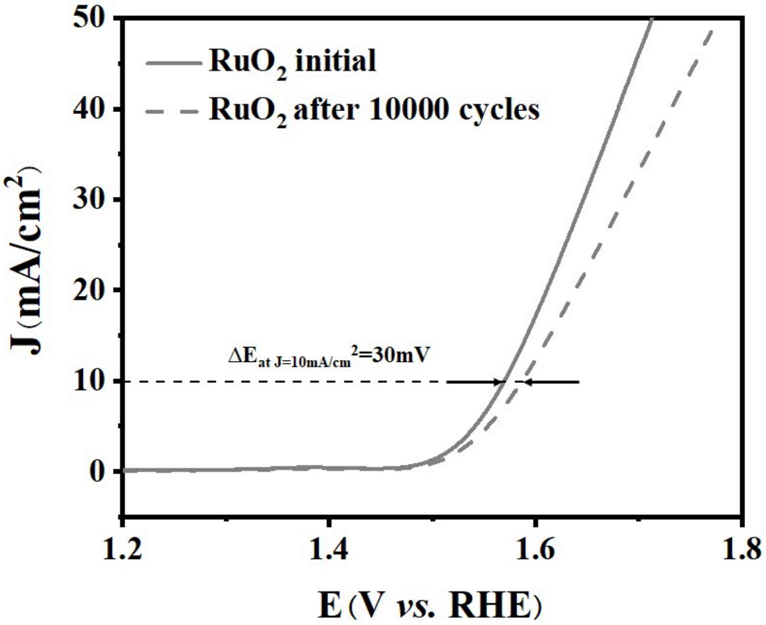

Fig. S17. OER polarization curves of the RuO_2 before and after 10000 potential cycles between 1.4 and 1.8 V versus RHE with a scan rate of 50 mV s^{-1} in O_2-saturated 0.1 M KOH solution.

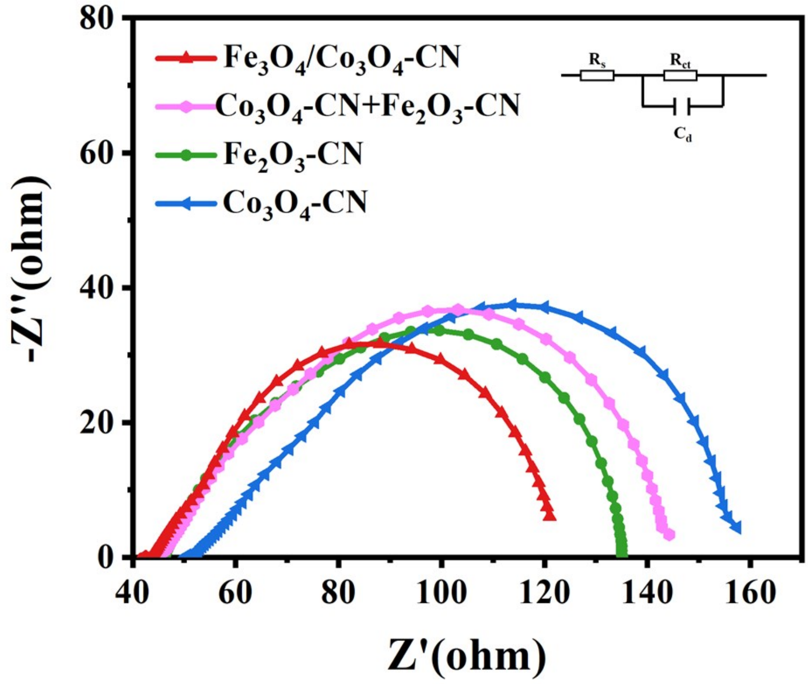

Fig. S18. Nyquist plots for Fe_3O_4/Co_3O_4-CN, Fe_2O_3-CN+Co_3O_4-CN, Co_3O_4-CN and Fe_2O_3-CN.

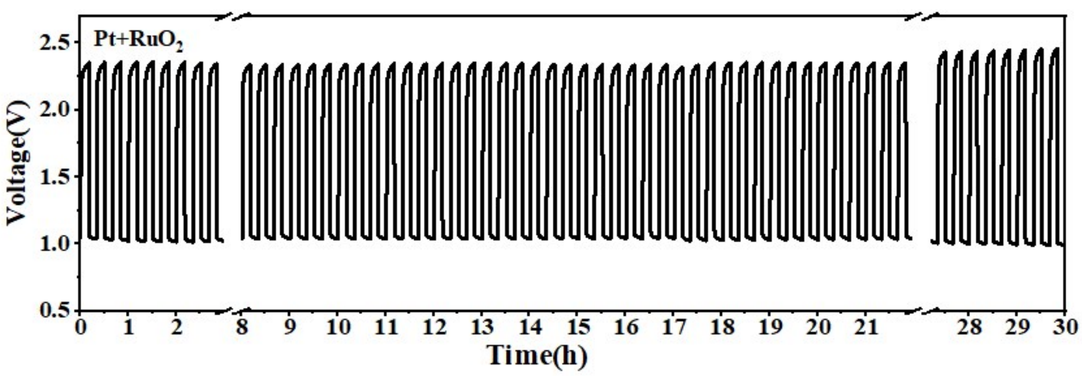

Fig. S19. Cycling performance at the charging and discharging current density of 10 mA cm^{-2} of the ZnAB battery with Pt/C+RuO_2 as the air cathode catalyst.

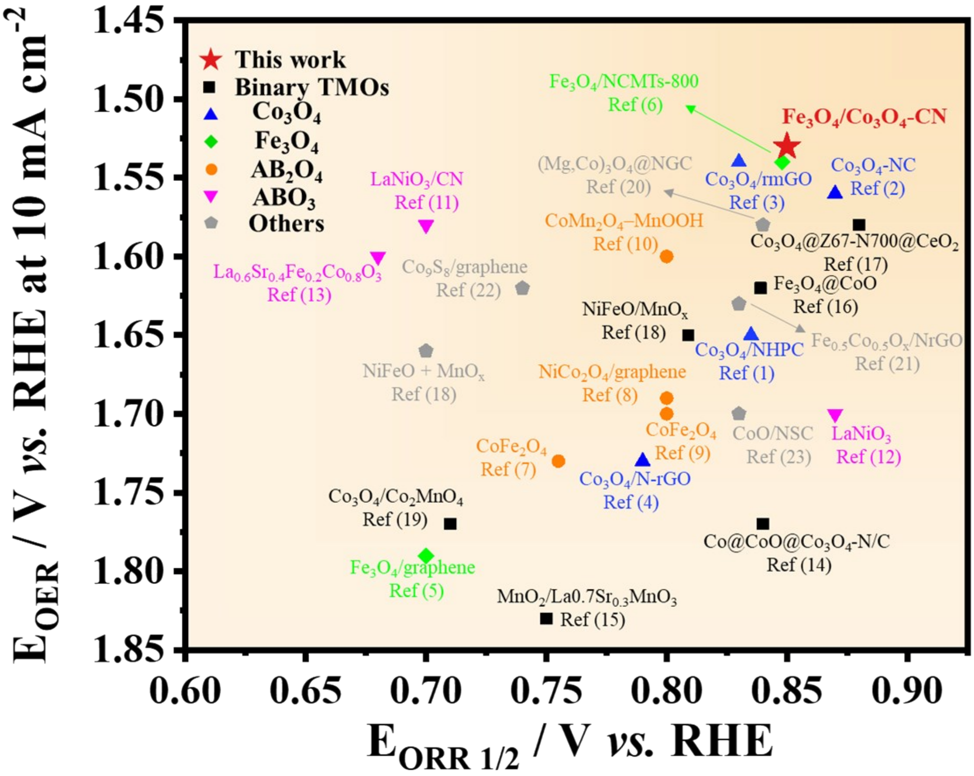

Fig. S20. Comparison of ΔE of Fe_3O_4/Co_3O_4-CN with other reported bifunctional metal oxide-based catalysts in literatures.

Table S1. The BET surface area and pore size distribution of catalysts.

Catalysts	**BET (m^2 g^{-1})**			
	Micro-pores (<2nm)	Meso-/macro-pores (2-100nm)	surface area	(meso-/macro-pores)/micro-pores
	Area	Area		
Fe_3O_4/Co_3O_4-CN	462	546	1008	1.18
Co_3O_4-CN	502	257	795	0.51
Fe_2O_3-CN	762	558	1320	0.73
CN	744	436	1180	0.59

Table S2. The detailed binding energies and integrated areas of Co 2p, Fe 2p, N 1s and O 1s peaks of the samples.

		Fe_3O_4/Co_3O_4-CN		**Co_3O_4-CN**		**Fe_2O_3-CN**	
		position	area	position	area	position	area
Co	Co^{2+}	782.36	468.78	781.51	782.12	-	-
	$Co^{2+'}$	797.21	242.93	796.63	378.21	-	-
	Co^{3+}	779.88	1231.91	779.77	636.69	-	-
	$Co^{3+'}$	794.88	638.41	794.93	405.31	-	-
Fe	Fe^{2+}	709.74	447.09	-	-	709.57	106.74
	$Fe^{2+'}$	722.50	298.83	-	-	722.34	58.35
	Fe^{3+}	711.33	673.99	-	-	710.89	357.71
	$Fe^{3+'}$	725.31	244.89	-	-	725.47	157.31
O	O_a	530.15	2624.68	529.80	4039.84	529.88	3828.53
	O_b	531.83	2372.23	531.34	1325.69	531.52	1453.29
	O_c	533.04	1132.44	532.81	734.33	532.90	929.81
N	Pyri-N	398.42	1517.21	398.12	1545.14	398.16	630.80
	Pyrr-N	399.92	326.88	399.77	1078.31	399.84	646.11
	Grap-N	400.95	1035.37	400.81	832.96	401.05	372.68
	Oxid-N	403.11	218.98	403.47	139.28	403.30	90.47

The molar percentage of Fe^{2+} and Co^{2+} are calculated by using

$$[Fe^{2+}] = \frac{A_{Fe^{2+}} + A_{Fe^{2+'}}}{A_{Fe^{2+}} + A_{Fe^{2+'}} + A_{Fe^{3+}} + A_{Fe^{3+'}}}$$

$$[Co^{2+}] = \frac{A_{Co^{2+}} + A_{Co^{2+'}}}{A_{Co^{2+}} + A_{Co^{2+'}} + A_{Co^{3+}} + A_{Co^{3+'}}}$$

where A is the integrated area of metal ion (Fe^{2+}, Fe^{3+}, Co^{2+} and Co^{3+}) peak shown in Table S2.

Table S3. Potential differences comparison of Fe_3O_4/Co_3O_4-CN with previously reported bifunctional catalysts.

	Catalyst material	Mass loading / mg cm^{-2}	$E_{ORR\ 1/2}$ / $V_{vs.}$ RHE	$E_{OER\ j=10}$ / $V_{vs.}$ RHE	ΔE ($E_{OER\ j=10}$ - $E_{ORR\ 1/2}$)	Ref.
Our Sample	Fe_3O_4/Co_3O_4-CN	0.2	0.85	1.53	0.68	This work
Co_3O_4	Co_3O_4/NHPC	0.2	0.835	1.65	0.81	1
	Co_3O_4-NC	1.2	0.87	1.56	0.68	2
	Co_3O_4/rmGO	-	0.83	1.54	0.69	3
	Co_3O_4/N-rGO	0.12	0.79	1.73	0.93	4
Fe_3O_4	Fe_3O_4/graphene	0.2	0.7	1.79	1.09	5
	Fe_3O_4/NCMTs-800	0.1	0.848	1.54	0.7	6
AB_2O_4	$CoFe_2O_4$	-	0.755	1.73	0.87	7
	$NiCo_2O_4$/graphene	0.4	0.8	1.69	0.99	8
	$CoFe_2O_4$	0.1	0.8	1.7	0.9	9
	$CoMn_2O_4$–MnOOH	-	0.8	1.6	0.8	10
ABO_3	$LaNiO_3$/CN	0.1	0.7	1.58	0.88	11
	$LaNiO_3$	0.78	0.87	1.7	0.85	12
	$La_{0.6}Sr_{0.4}Fe_{0.2}Co_{0.8}O_3$	0.2	0.68	1.6	0.95	13
Binary TMOs	Co@CoO@Co_3O_4-N/C	0.25	0.84	1.77	0.92	14
	$MnO_2/La_{0.7}Sr_{0.3}MnO_3$	0.23	0.75	1.83	1.04	15
	Fe_3O_4@CoO	0.3	0.839	1.62	0.77	16
	Co_3O_4@Z67-N700@CeO_2	0.126	0.88	1.58	0.68	17
	NiFeO/MnO_x	0.1	0.8	1.63	0.83	18
	Co_3O_4/Co_2MnO_4	0.2	0.71	1.77	1.03	19
Others	$(Mg,Co)_3O_4$@NGC	0.3	0.842	1.58	0.73	20
	NiFeO + MnO_x	0.1	0.809	1.613	0.793	18
	$Fe_{0.5}Co_{0.5}O_x$/NrGO	0.5	0.83	1.63	0.78	21
	Co_9S_8/graphene	0.2	0.74	1.62	0.86	22
	CoO-NSC	-	0.83	1.70	0.88	23

References

1 J. Guan, Z. Zhang, J. Ji, M. Dou, F. Wang, ACS Appl. Mater. Inter., 2017, **9**, 30662-30669.

2 C. Guan, A. Sumboja, H. Wu, W. Ren, X. Liu, H. Zhang, Z. Liu, C. Cheng, S.J. Pennycook, J. Wang, Adv. Mater., 2017, **29**, 1704117.

3 Y. Liang, Y. Li, H. Wang, J. Zhou, J. Wang, T. Regier, H. Dai, Nat. Mater., 10 2011 780-786.

4 F. Cheng, T. Zhang, Y. Zhang, J. Du, X. Han, J. Chen, Enhancing electrocatalytic oxygen reduction on MnO_2 with vacancies, Angew. Chem. Int. Ed., 2013, **52**, 2474-2477.

5 B. Zhao, Y. Zheng, F. Ye, X. Deng, X. Xu, M. Liu, Z. Shao, ACS Appl. Mater. Inter., 2015, **7**, 14446-14455.

6 G. Liu, B. Wang, P. Ding, Y. Ye, W. Wei, W. Zhu, L. Xu, J. Xia, H. Li, J. Alloy. Compd., 2019, **797**, 849-858.

7 W. Bian, Z. Yang, P. Strasser, R. Yang, J. Power Sources, 2014, **250**, 196-203.

8 D.U. Lee, B.J. Kim, Z. Chen, J. Mater. Chem. A, 2013, **1**, 4754-4762.

9 A. Indra, P.W. Menezes, N.R. Sahraie, A. Bergmann, C. Das, M. Tallarida, D. Schmeißer, P. Strasser, M. Driess, J. Am. Chem. Soc., 2014, **136**, 17530-17536.

10 Y. Wang, T. Hu, Q. Liu, L. Zhang, Chem. Commun., 2018, **54**, 4005-4008.

11 W.G. Hardin, D.A. Slanac, X. Wang, S. Dai, K.P. Johnston, K.J. Stevenson, J. Phys. Chem. Lett., 2013, **4**, 1254-1259.

12 D.U. Lee, H.W. Park, M.G. Park, V. Ismayilov, Z. Chen, ACS Appl. Mater. Inter., 2015, **7**, 902-910.

13 K. Elumeeva, J. Masa, J. Sierau, F. Tietz, M. Muhler, W. Schuhmann, Electrochim. Acta, 2016, **208**, 25-32.

14 G. Xu, G.C. Xu, J.J. Ban, L. Zhang, H. Lin, C.L. Qi, Z.P. Sun, D.Z. Jia, J. Colloid Interf. Sci., 2018, **521**, 141-149.

15 S. Yan, Y. Xue, S. Li, G. Shao, Z. Liu, ACS Appl. Mater. Inter., 2019, **11**, 25870-25881.

16 L. Zhou, B. Deng, Z. Jiang, Z.J. Jiang, Chem. Commun., 2019, **55**, 525-528.

17 X. Li, S. You, J. Du, Y. Dai, H. Chen, Z. Cai, N. Ren, J. Zou, J. Mater. Chem. A, 2019, **7**, 25853-25864.

18 J. Guan, Z. Zhang, J. Ji, M. Dou, F. Wang, ACS Appl. Mater. Inter., 2017, **9**, 30662-30669.

19 D. Wang, X. Chen, D.G. Evans, W. Yang, Nanoscale, 2013, **5**, 5312-5315.

20 Y.P. Deng, Y. Jiang, D. Luo, J. Fu, R. Liang, S. Cheng, Z. Bai, Y. Liu, W. Lei, L. Yang, ACS Energy Lett., 2017, **2**, 2706-2712.

21 L. Wei, H.E. Karahan, S. Zhai, H. Liu, X. Chen, Z. Zhou, Y. Lei, Z. Liu, Y. Chen, Adv. Mater., 2017, **29**, 1701410.

22 S. Dou, L. Tao, J. Huo, S. Wang, L. Dai, Energ. Environ. Sci., 2016, **9**, 1320-1326.

23 S. Chen, S. Chen, B. Zhang, J. Zhang, ACS Appl. Mater. Inter., 2019, **11**, 16720-16728.